

A Novel Inverter for Single Phase Drive and Grid-Connected Solar Systems

V Kumar Reddy Majji

Assistant Professor

Department of Electrical and Electronics Engineering
Aditya College of Engineering, Surampalem, Andhra Pradesh India

Abstract: The grid tied photovoltaic system suffers a great loss because the performance of the transformer present in the inverter. The cost of the transformer is high and the maintenance cost is also high. Therefore transformerless inverter are widely used in grid tied photovoltaic system, due to the benefits of achieving high efficiency and low cost. The sinusoidal pulse width modulation of full bridge transformerless inverters can achieve high efficiency by using metal oxide semiconductor field effect transistor. Various topology has been implemented for transformerless inverter, but in that there is a problem of losses and reverse recovery characteristics. In our paper we are going to implement the center tapped H bridge transformerless inverter topology for grid tied photovoltaic system to avoid the losses and leakage current. A clamped branch is added in the transformerless inverter. The added clamping branch clamps the freewheeling voltage at the freewheeling period. As the common mode voltage is kept constant for the whole grid period that reduces the leakage current. The splitting structure of inductor at the region of grid side avoids reverse recovery voltage and this improves the efficiency of the system. The detailed analysis of our topology with the operational modes, leakage current analysis and design consideration were implemented and the proposed inverter is applied for single phase induction motor.

Keywords: common mode voltage, inverter, Photovoltaic (PV) grid-connected system, PWM control, transformerless, leakage current.

I. Introduction:

Transformer less inverters are widely used in grid-tied photovoltaic (PV) generation systems, due to The benefits of achieving high efficiency and low cost. Various transformerless inverter topologies have been Proposed to meet the safety requirement of leakage currents, when no transformer is used in a grid connected Photovoltaic system, a galvanic connection between the grid and PV array exists. In these conditions, dangerous Leakage currents (common-mode currents) can appear through the stray capacitance between the PV array and the ground. In order to avoid these leakage currents, different inverter topologies that generate no varying common-mode voltages have been proposed.

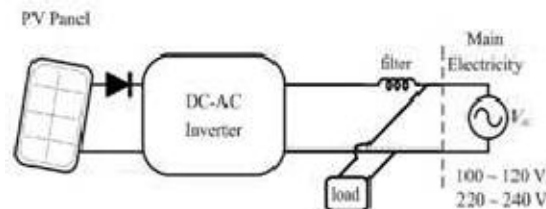
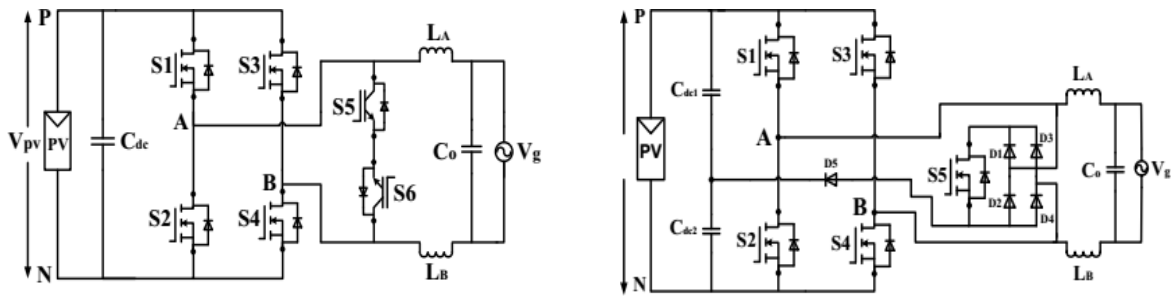


Fig.1 Schematic diagram of PV panel connected to Grid connected loads

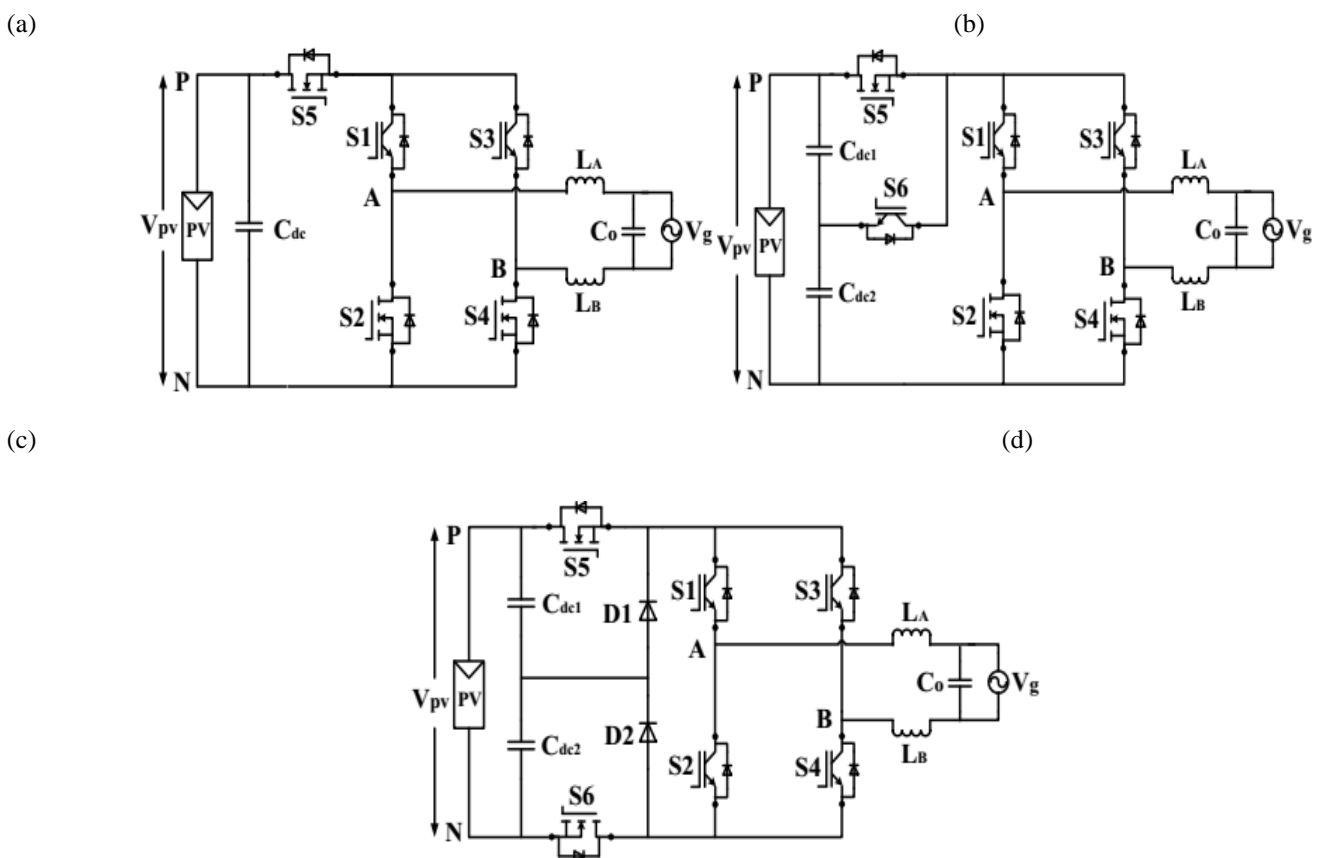
The CM voltage needs to be clamped to the mid-point of dc input voltage instead of only disconnecting the PV module from the grid. On the other hand, to improve the efficiency, transformerless inverter can be implemented using super-junction MOSFET and SiC diodes. The super-junction MOSFETs can avoid the fixed voltage drop and turn-off losses caused by tail current, thereby reducing the conduction and switching losses.

However, due to poor reverse recovery of MOSFETs slow body-diode, it is limited to use in transformerless inverter. In the following, MOSFET based transformerless topologies for grid-tied PV application will be reviewed and discussed based on their circuit structure, efficiency and CM voltage clamping capability.

The most attractive transformerless topology is the Highly Efficient and Reliable Inverter Concept (HERIC) topology which is shown in Fig.1(a). This topology has been implemented in some commercial inverters, especially those from Sunway's converter. Two switches are added in the ac side of full-bridge (FB) topology to decouple the PV module from the grid during the freewheeling period. Though the PV module is decoupled from the grid, a fluctuating CM voltage could be observed because the



freewheeling path potential is not clamped at the half of dc input voltage. As seen in Fig.1(b), the topology which has been proposed in [10] replaces the two switches freewheeling branch with one bi-directional switch and four diodes called H-bridge zero voltage rectifier (HB-ZVR) topology. Also, another diode (D5) has been added for better eliminating the leakage current. The clamping function of this topology has been done using D5 which allows one-directional clamping, only if the freewheeling path potential ($V_{AN} \approx V_{BN}$) is higher than the dc link mid-point voltage. As a result, CM voltage fluctuation could be observed when the reverse condition is occurred which is very less than HERIC topology. In these two topologies, the grid current flows through two switches during the whole grid period; as a result, conduction loss is low.



(a) HERIC topology proposed in [12]

(b) HB-ZVR topology proposed in [10] (c) H5 topology proposed in [157] (d) oH5 topology proposed in [9] (e) H6 topology [20] Fig.1(c) shows another explicit transformerless topology proposed called H5 topology, made up by adding an extra switch in the dc side of FB inverter. In this topology, the freewheeling current flows through S_1 and body diode of S_3 during positive half cycle, and S_3 and body diode of S_1 during negative half cycle. As a result, the switches S_1 and S_3 could not be implemented with MOSFETs due to the low reverse recovery of the MOSFET body diode. Another disadvantage is that the output current flows through three switches in the active mode for the complete grid cycle, thus higher conduction losses are present. A fluctuating CM voltage could also be observed because the freewheeling path potential is not clamped at the mid-point of dc link. An extension of H5 topology is presented called optimized H5 (oH5) topology, where an extra switch (S6) has been added with the H5 topology to clamp the CM voltage at the half of input voltage as demonstrated in Fig.3.1(d). Unfortunately, a dead time must have to be added between the gate signals of the switches S_5 and S_6 to avoid the short circuit of the input split capacitor C_{dc1} . As a result, CM voltage fluctuates in dead time [9]. Another disadvantage of this topology is that higher conduction losses still remain due to the grid current flows through three switches in the active mode. Gonzalez et al. proposed another topology in [16] called full-bridge with dc bypass (FB-DCBP) which is also named as H6 topology. It employs two switches and two diodes in the dc side of FB inverter. The CM characteristics of this topology are

better than other topologies because of the bi-directional clamping branch. During freewheeling mode, either diode D1 or D2 can be conducted based on whether the freewheeling path potential ($V_{AN} \approx V_{BN}$) is higher or lower than half of the dc link voltage. In this topology, leakage current removal effect depends only on the turn-on speed of the clamping diodes. However, this topology can be implemented with two MOSFET switches (S5 & S6) only. In addition, the grid current flows through four switches, thus higher conduction losses are also present.

Considering the advantages and the drawbacks of the transformerless inverter mentioned earlier, a family of new transformerless topologies for single-phase grid-tied PV system is proposed based on two asymmetric phase legs in this work. The key features of the proposed inverter are: (1) no dead time is required because the switches in the same phase-leg are never all turned-on during the same SPWM cycle; as a result, current distortion at output is lower, (2) the CM voltage is kept constant at the half of dc input voltage because of the added clamping branch, (3) during the positive and negative half cycle, the inductor current flows through two and three switches respectively, thus the conduction loss is lower. The detailed operation principles and the control scheme to reduce the dc current injection are described. An investigation has been conducted to calculate the device power losses and to make a detail comparison with the topologies presented in Fig.1.

II. Proposed Topology and Modulation Strategy:

A. Derivation method of the proposed topology

The traditional MOSFET based phase legs of transformerless inverter are shown in Fig.2 (a) & (b). In order to ensure high efficiency, a modification is made in Fig.2(a)& (b) by replacing IGBTs with MOSFETs and diodes which is shown in Fig.2(c) & (d). By combining these two-phase legs, a family of new transformerless topologies is derived based on the ac decoupling and asymmetric phase legs. The followings are the derivation steps of the proposed new topologies:

First, IGBT switches of the HERIC and H5 methods are replaced with MOSFETs and diodes to boost the efficiency.

Next, combine these two-phase legs to derive new topology. By changing the position of the free wheeling's witches (S3 & D1), the family of the new topologies is derived.

Finally, to clamp the CM voltage at the half of the DC input voltage, a clamping branch consisting of a switch and a diode with a capacitor divider is introduced.

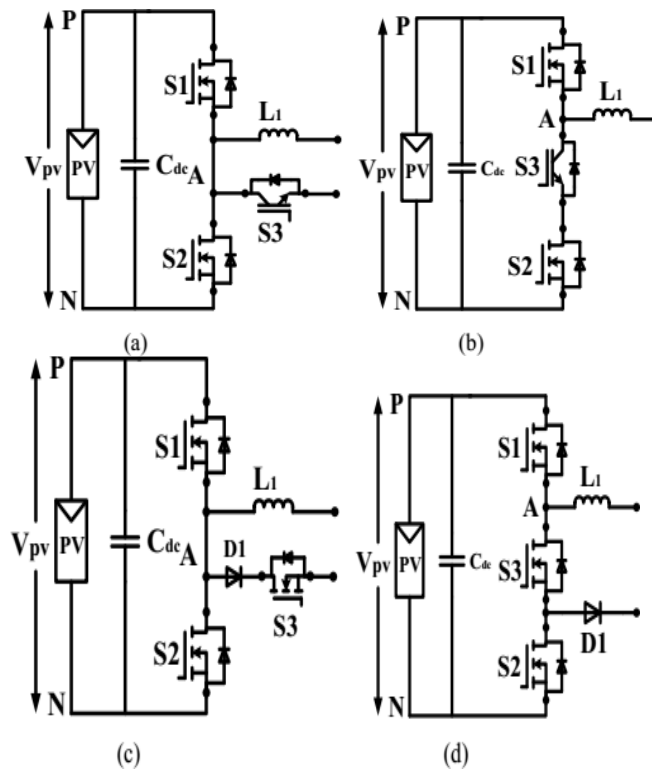


Fig..2. MOSFET based phase legs for transformerless inverter: (a) HERIC method (b) H5 method (c) modification of HERIC method (d) modification of H5 method

B. Circuit Configuration

The family of the proposed transformerless PV inverter topology is depicted in Fig.3 which is derived according to the derivation method described in the prior section, where S1,S2, S4, & S5 are high frequency switches, and S3 & S6 are low frequency freewheeling switches. The unidirectional clamping branch is constructed using switch S7 and diode D3 with a capacitor divider (C_{dc1} & C_{dc2}) which clamps the CM voltage at the midpoint of dc link. LA, LB, and Co make up the LC type filter connected to the grid and Vpv represent the input dc voltage. The unipolar SPWM can be employed to the proposed topology with three-level output voltage. The MOSFET power switches are utilized as no reverse-recovery issues are required for the proposed

configuration of the inverter for unity power factor operation. Consequently, the efficiency of the entire PV system is increased.

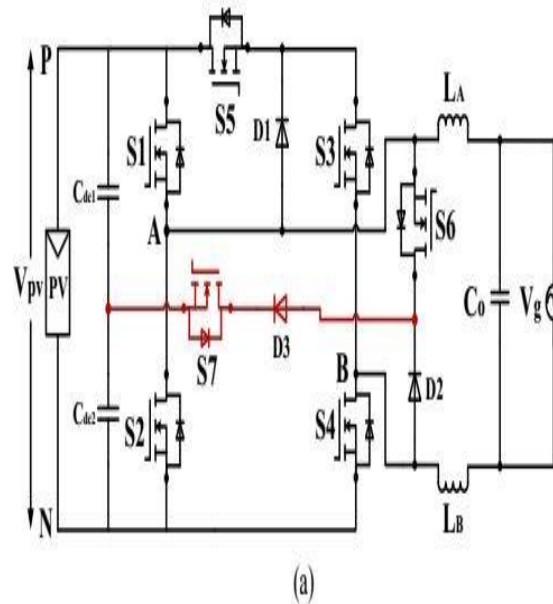


Fig.3. family of the proposed transformerless grid connected PV inverter topologies: (a) circuit structure A

C. Operating Principle

In order to analysis and verify, the circuit structure A is taken as an example. Fig.4 shows the switching pattern for unity power factor operation, where the G1, G2, G3, G4, G5, G6, and G7 are the gate signals of the switches S1, S2, S3, S4, S5, S6, and S7. As can be seen, (S1, S4) and (S2, S5) commutate at the switching frequency with the identical commutation order in the positive and negative half cycle of the grid current, respectively. In Fig.3.5, the operating principles of the proposed topology are shown. Four operation modes are proposed to generate the output voltage state of +V_{PV}, 0, and -V_{PV}, which can be explained as follows:

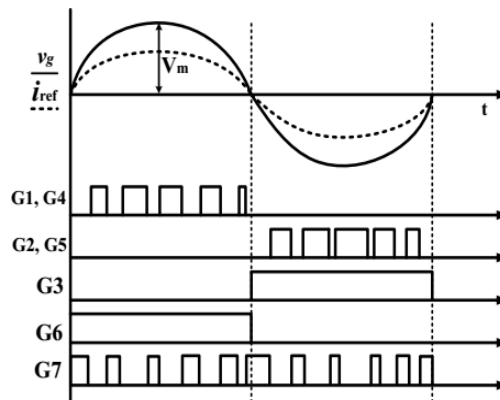


Fig.4. Gate drive signals of the proposed topology for circuit structure A

Mode 1 is the active mode in the positive half cycle of the grid current. When S1 and S4 are turned-on, the inductor current i_L increases linearly through grid. In this mode, $V_{AN} = V_{PV}$ and $V_{BN} = 0$, thus $V_{AB} = V_{PV}$ and the inductor current:

$$(1) \quad i_L(t) = \frac{V_{PV} - v_g(t)}{L}$$

Mode 2 is the freewheeling mode in the positive half cycle of the grid current, as indicated in Fig.5(b). The inductor current i_L flows through S6 and D2, and reduces linearly under the effect of grid voltage. In this state, V_{AN} falls and V_{BN} rises until their values are equal. If the voltages ($V_{AN} \approx V_{BN}$) are higher than half of the dc link voltage, freewheeling current flows through S7 and D3 to the mid-point of the dc link, results V_{AN} and V_{BN} are clamped at $V_{PV}/2$. Therefore, at mode 2, $V_{AN} = V_{PV}/2, V_{BN} = V_{PV}/2$, the inverter output voltage $V_{AB} = 0$ and the inductor current:

$$(2) \quad i_L(t) = \frac{-v_g(t)}{L}$$

Mode 3 is the active mode in the negative half cycle of grid current. Similar to mode 1, when S2, S3 and S5 are turned-on, the inductor current increases in the opposite direction. In this mode, the voltage $V_{AN} = 0$ and $V_{BN} = V_{PV}$, thus $V_{AB} = -V_{PV}$ and the inductor current:

$$i_L(t) = \frac{V_{PV} - v_g(t)}{L} (t)$$

(3)

Mode 4 is the freewheeling mode in the negative half cycle of grid current. When S5 and S2 are turned-off, the inductor current flows through S3 and D1. Similar to mode 2, If the voltages ($V_{AN} \approx V_{BN}$) are higher than half of the dc link voltage, freewheeling current flows through S7 and D3 to the mid-point of the dc link, results the voltages V_{AN} and V_{BN} are clamped at $V_{PV} / 2$. Therefore, in this mode, $V_{AN} = V_{BN} = V_{PV} / 2$, $V_{AB} = 0$, and the inductor current:

$$i_L(t) = \frac{-v_g(t)}{L} (t)$$

freewheeling path potential is clamped at the mid-point of the dc link during freewheeling period of positive and negative half cycle. As a result, the inverter hardly generates any leakage current. It can also be seen that the anti-parallel diodes of the MOSFETs remained inactive during the whole operation period. Therefore, the proposed topology could be implemented utilizing MOSFET switches. However, the body-diode will be activated if a phase shift is occurred in the inverter output voltage and current. Accordingly, the dependability of the system will be reduced because of the MOSFET anti-parallel diode low reverse recovery issues.

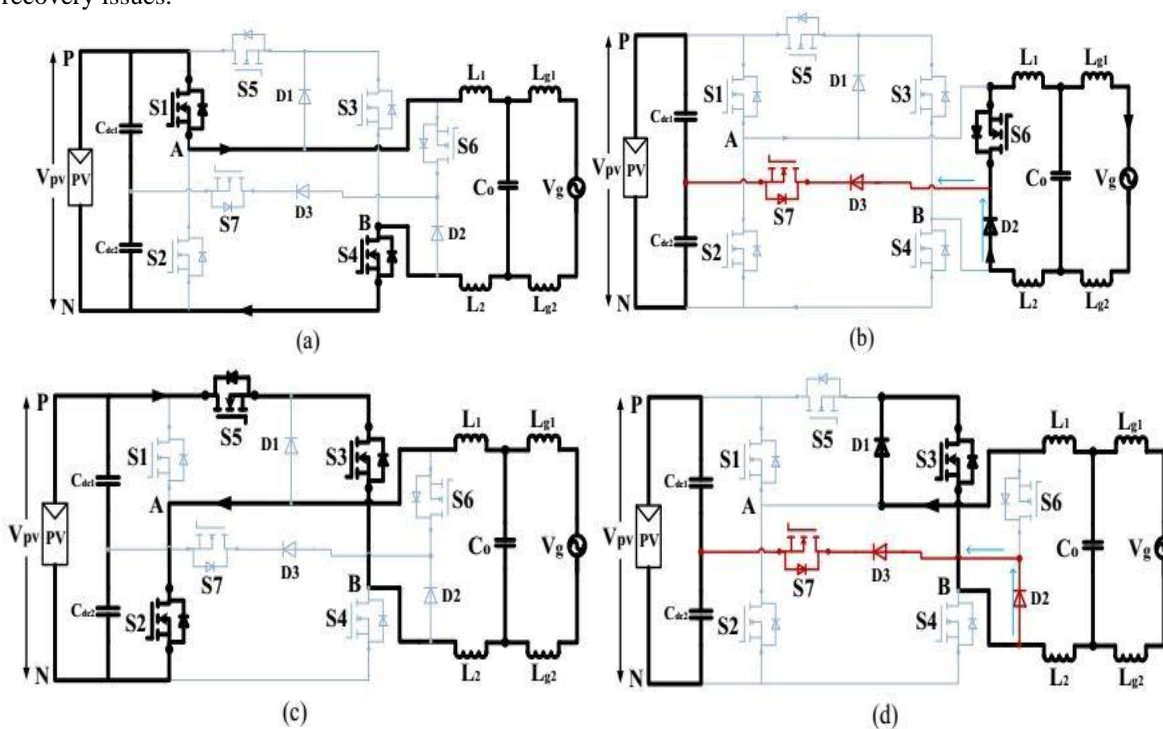


Fig.5. Operating principle of the proposed topology: (a) active and (b) freewheeling modes in the positive half cycle of the grid current; (c) active and (d) freewheeling modes in the negative half cycle of the grid current.

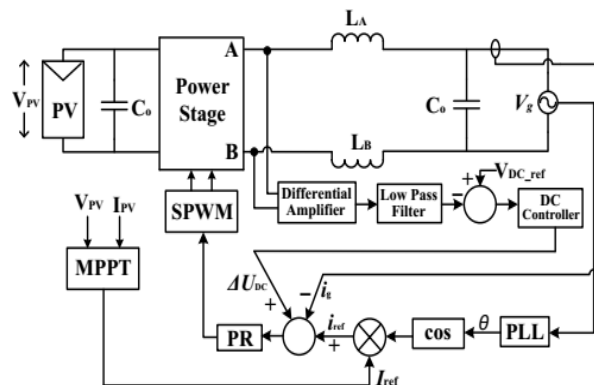


Fig.6. Control block of the proposed topology

D. Control Technique

In case of transformerless inverter, dc current injection into the utility grid is an important issue that may cause saturation of distribution transformer, increased loss, and abnormal operation of the load connected to the grid. In order to suppress the dc

current injection into the utility grid, several control strategies have been investigated in the literature. Based on the control technique proposed an improved control strategy as depicted in Fig.6, is implemented to control the proposed topology. The control block consists of a dc suppression loop, a grid current controller, and a phase locked loop to synchronize with the grid current. The dc suppression loop is composed of a differential amplifier, a low pass filter and a dc controller. Since the output of the low pass filter of dc suppression loop is constant in steady state, so a proportional integral (PI)controller is used to control the dc offset voltage. On the other hand, grid current is sinusoidal and the proportional resonant (PR) controller has better performance of tracking the reference signal if compared to the normal PI controller and repetitive controller (RC). Therefore, if compared with the control scheme proposed a PR controller is selected to control the grid current of the proposed topology. The block diagram of the PR controller and dc suppression loop is shown in Fig.7, where GPR(s), Gd(s) and GPI(s) are the transfer function of fundamental current controller, processing and PWM delay, and offset voltage controller, respectively. The transfer functions are given below:

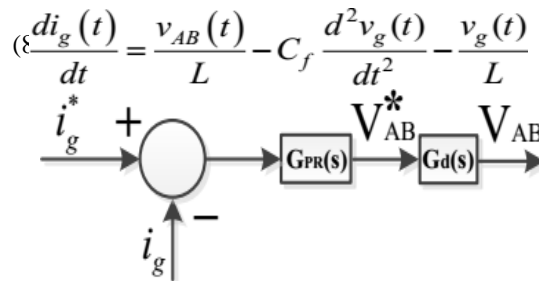
$$G_{PR}(s) = K_{pi} + K_{ii} * \frac{s}{s^2 + \omega_f^2}$$

$$G_d(s) = \frac{1}{1 + 1.5T_s s}$$

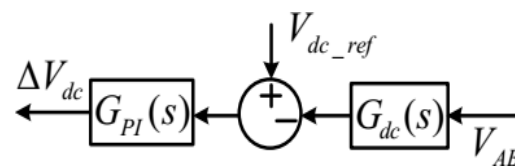
$$G_{PI}(s) = K_{pdc} + K_{idc} * \frac{1}{s}$$

(7)

Where Kpi and Kii are the proportional and integral gain of the offset voltage controller, ωf is the fundamental frequency, and Ts is the sampling period. Since an LC filter (LCf) has been used as output filter, thus the system at ac side can be described as follows:



(a)



(b)

Fig.7. (a) Block diagram of PR controller (b) Block diagram of the DC suppression loop In Laplace domain, equation (8) can be rewritten as

$$I_g(s) = \frac{V_{AB}(s)}{Ls} - C_f s^2 V_g(s) - \frac{V_g(s)}{Ls}$$

(9)

Wherein and vg are grid current and voltage, VAB is the inverter output voltage. Consequently, the equivalent model of the output filter can be drawn as Fig.8.

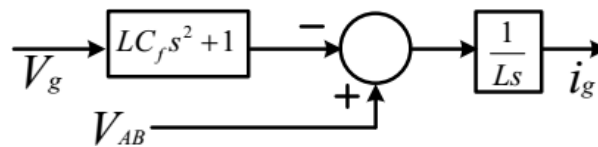


Fig.8. Equivalent model of the output filter in Laplace domain

Henceforth, according to the above illustration, the overall control diagram can be depicted as shown in Fig.9, where Gdc(s) is the feedback gain of the dc suppression loop.

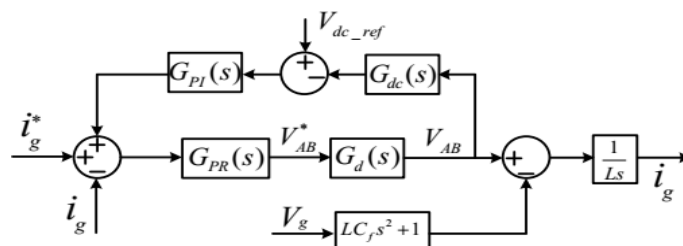


Fig.9. The complete control diagram of the proposed topology in Laplace domain

III. Leakage Current Analysis and Power Devices Loss Calculation:

A. Leakage Current Analysis for the Proposed Topology

The PV module generates an electrically chargeable surface area which faces a grounded frame. In case of such configuration, a capacitance is formed between the PV module and the ground. Since this capacitance occurs as an undesirable side effect, it is referred as parasitic capacitance. Due to the loss of galvanic separation between the PV module and the grid, a CM resonant circuit can be created. An alternating CM voltage that depends on the topology structure and control scheme, can electrify the resonant circuit and may lead to high ground leakage current. In order to analyze the CM characteristics, an equivalent circuit of the proposed topology as shown in Fig.10 can be drawn, where VAN, and VBN are the controlled voltage source connected to the negative terminal N, LCM and CCM are the CM inductor and capacitor, CPvg is the parasitic capacitance, and Zg is the grid impedance.

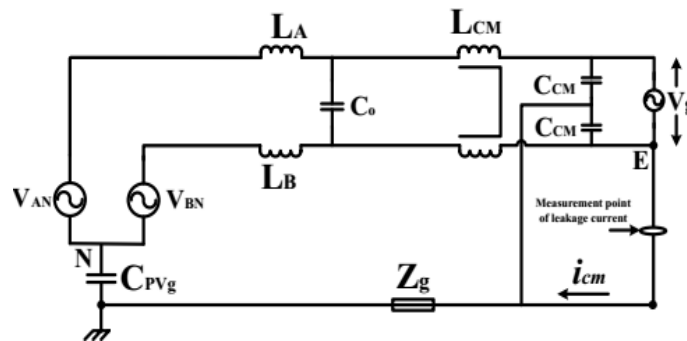


Fig.10. Equivalent CM model of the proposed topology According to the definition of common-mode (CM) and differential-mode (DM) voltage:

$$V_{CM} = \frac{1}{2}(V_{AN} + V_{BN}) \tag{10}$$

$$V_{DM} = V_{AN} - V_{BN} \tag{11}$$

where VCM and VDM are respectively the CM and DM voltages. Solving (10) and (11), VAN and VBN can be expressed as follows:

$$V_{AN} = V_{CM} + \frac{1}{2}V_{DM} \tag{12}$$

$$V_{BN} = V_{CM} - \frac{1}{2}V_{DM} \tag{13}$$

In order to illustrate the CM model at switching frequency the grid is a low frequency (50-60Hz) voltage source; thus the impact of grid on the leakage current can be neglected. The DM capacitor Co can also be removed since it has no effect on the leakage current. Consequently, the simplified high frequency CM model of the proposed topology could be drawn as Fig.11. The equation for the total CM voltage can easily be derived from Fig.3.11 as:

$$V_{tCM} = V_{CM} + \frac{V_{DM}}{2} \frac{L_B - L_A}{L_A + L_B} \tag{14}$$

Where VtCM represent total CM voltage of the proposed topology is derived in Fig.12. In the proposed inverter if LA = LB for a well-designed circuit with symmetrically structured magnetic, equation (14) can be rewritten as follows:

$$V_{tCM} = V_{CM} = \frac{1}{2}(V_{AN} + V_{BN}) = \text{constant} \tag{15}$$

$$\text{Mode 1: } V_{tCM} = \frac{1}{2}(V_{AN} + V_{BN}) = \frac{1}{2}(V_{PV} + 0) = \frac{1}{2}V_{PV} \tag{16}$$

$$\text{Mode 2: } V_{tCM} = \frac{1}{2}(V_{AN} + V_{BN}) = \frac{1}{2}\left(\frac{1}{2}V_{PV} + \frac{1}{2}V_{PV}\right) = \frac{1}{2}V_{PV} \tag{17}$$

$$\text{Mode 3: } V_{tCM} = \frac{1}{2}(V_{AN} + V_{BN}) = \frac{1}{2}(0 + V_{PV}) = \frac{1}{2}V_{PV} \tag{18}$$

$$\text{Mode 4: } V_{ICM} = \frac{1}{2}(V_{AN} + V_{BN}) = \frac{1}{2}\left(\frac{1}{2}V_{PV} + \frac{1}{2}V_{PV}\right) = \frac{1}{2}V_{PV}$$

(19)
 It is clear from equations (16)-(19) that the total CM voltage for the proposed topology during the whole operation period is kept constant at $V_{PV}/2$. Therefore, the ground leakage current is reduced significantly.

IV. Simulation Results:

A. Grid tied inverter

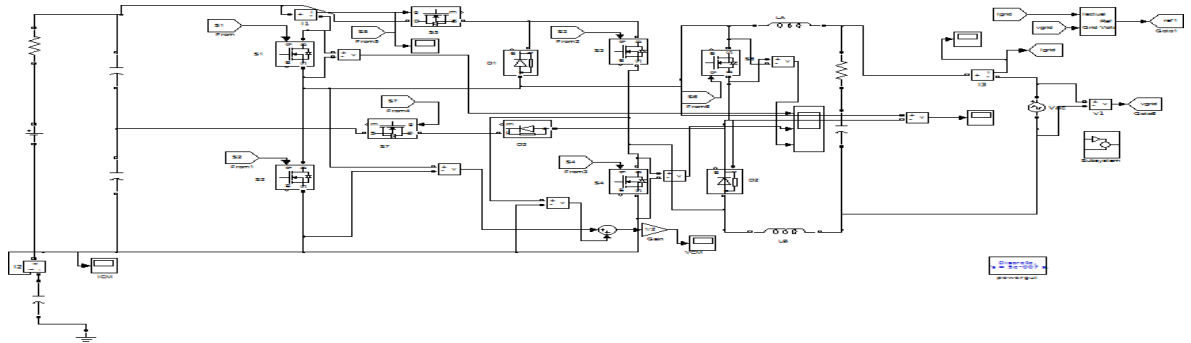


Fig.10 Matlab/Simulink model of Grid Tied inverter

B. Induction Motor Load

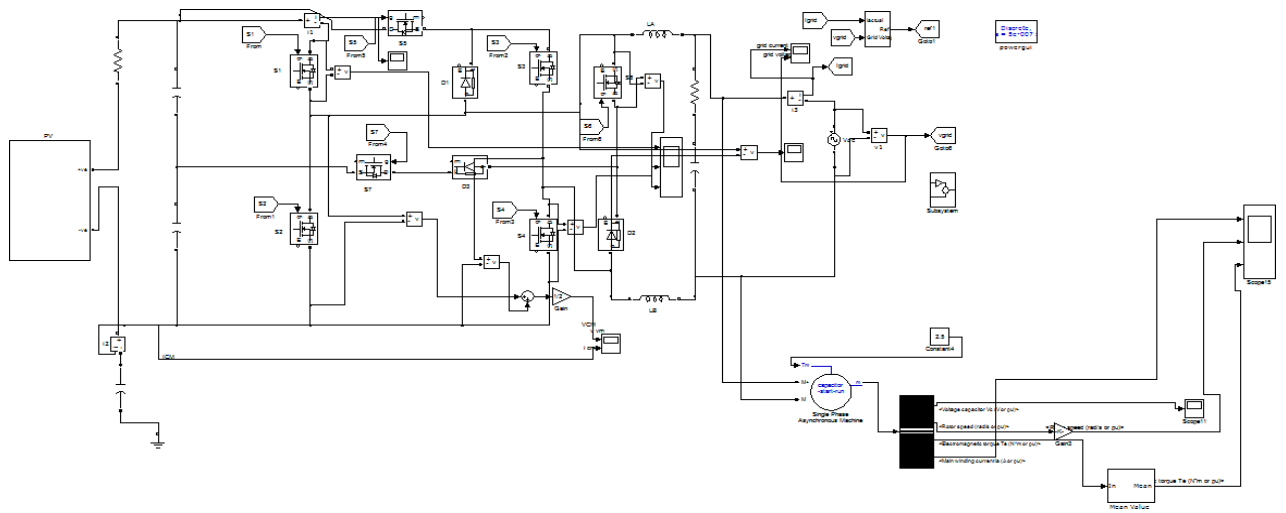


Fig.11 Matlab/Simulink Model of Induction motor Load

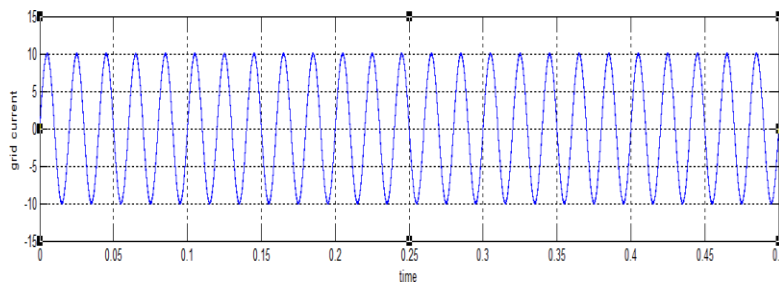


Fig.12 output grid current

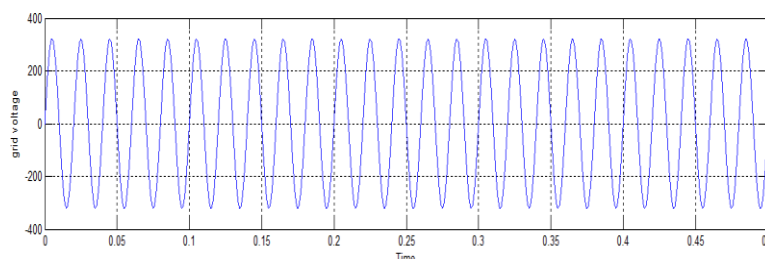


Fig.13 output grid voltage

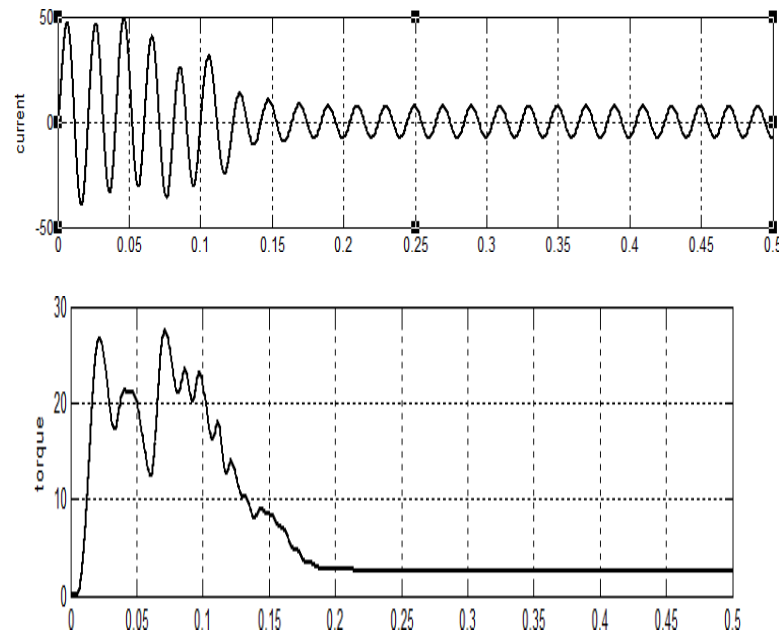
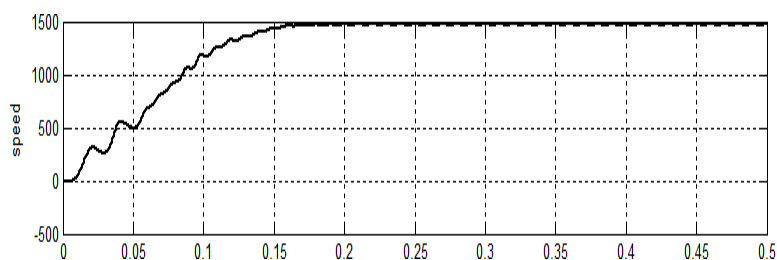


Fig.14 induction motor transient state and steady state characteristics. 1) current. 2) speed. And 3) torque



Conclusion:

In this paper, a family of new efficient transformerless inverter for grid-tied photovoltaic power generation system is presented using super-junction MOSFETs as main power switches. The main advantages of the proposed topology are as follows: (1) High efficiency over a wide load range is achieved by using MOSFETs and SiC diodes, (2) Like as isolated full-bridge inverter, excellent DM characteristics are achieved with uni polar SPWM, (3) PWM dead time is not required for main power switches, results low distortion at output. Therefore, it can be concluded that the proposed inverter is very suitable for a single-phase grid-tied PV application.

REFERENCES:

1. M. Islam, S. Mekhilef, and M. Hasan, "Single phase transformerless inverter topologies for grid-tied photovoltaic system: A review," *Renewable and Sustainable Energy Reviews*, vol. 45, pp. 69-86, 2015.
2. I. Patrao, E. Figueres, F. González-Espín, and G. Garcerá, "Transformerless topologies for grid-connected single-phase photovoltaic inverters," *Renewable and Sustainable Energy Reviews*, vol. 15, pp. 3423-3431, 2011.
3. Z. Li, S. Kai, F. Lanlan, W. Hongfei, and X. Yan, "A Family of Neutral Point Clamped Full-Bridge Topologies for Transformerless Photovoltaic Grid-Tied Inverters," *IEEE Transactions on Power Electronics*, vol. 28, pp. 730-739, 2013.
4. M. Islam and S. Mekhilef, "H6-type transformerless single-phase inverter for grid-tied photovoltaic system," *IET Power Electronics*, vol. 8, pp. 636-644, 2015.
5. H. Xiao, X. P. Liu, and K. Lan, "Zero-Voltage-Transition Full Bridge Topologies for Transformerless Photovoltaic Grid Connected Inverter," *IEEE Transactions on Industrial Electronics*, vol. PP, pp. 1-1, 2014.
6. X. Huafeng, K. Lan, and L. Zhang, "A Quasi-Unipolar SPWM Full-Bridge Transformerless PV Grid-Connected Inverter with Constant Common-Mode Voltage," *IEEE Transactions on Power Electronics*, vol. PP, pp. 1-1, 2014.
7. J. Baojian, W. Jianhua, and Z. Jianfeng, "High-Efficiency Single Phase Transformerless PV H6 Inverter With Hybrid Modulation Method," *IEEE Transactions on Industrial Electronics*, vol. 60, pp. 2104-2115, 2013.
8. D. Barater, G. Buticchi, E. Lorenzani, and C. Concari, "Active Common-Mode Filter for Ground Leakage Current Reduction in Grid-Connected PV Converters Operating With Arbitrary Power Factor," *IEEE Transactions on Industrial Electronics*, vol. 61, pp. 3940-3950, 2014.
9. X. Huafeng, X. Shaojun, C. Yang, and H. Ruhai, "An Optimized Transformerless Photovoltaic Grid-Connected Inverter," *IEEE Transactions on Industrial Electronics*, vol. 58, pp. 1887-1895, 2011.
10. T. Kerekes, R. Teodorescu, P. Rodriguez, G. Vazquez, and E. Aldabas, "A New High-Efficiency Single-Phase

- Transformerless PV Inverter Topology," IEEE Transactions on Industrial Electronics, vol. 58, pp. 184-191, 2011
11. B. N. Alajmi, K. H. Ahmed, G. P. Adam, and B. W. Williams, "Single-Phase Single-Stage Transformer less Grid-Connected PV System," IEEE Transactions on Power Electronics, vol. 28, pp.2664-2676, 2013
 12. G. Bin, J. Dominic, L. Jih-Sheng, C. Chien-Liang, T. LaBella, andC. Baifeng, "High Reliability and Efficiency Single-PhaseTransformerless Inverter for Grid- Connected Photovoltaic Systems," IEEE Transactions on Power Electronics, vol. 28, pp.2235-2245, 2013.
 13. Y. Bo, L. Wuhua, G. Yunjie, C. Wenfeng, and H. Xiangning,"Improved Transformerless Inverter With Common-ModeLeakage Current Elimination for a Photovoltaic Grid-Connected Power System," IEEE Transactions on Power Electronics, vol. 27,pp. 752-762, 2012.
 14. B. Chen, B. Gu, L. Zhang, Z. U. Zahid, J.-S. Lai, Z. Liao, et al., "AHigh Efficiency MOSFET Transformerless Inverter for Non isolated Micro-inverterApplications," IEEE Transactions on Power Electronics, vol. PP, pp. 1-1, 2014.
 15. T. Freddy, N. A. Rahim, W. P. Hew, and H. S. Che, "Comparison and Analysis of Single-Phase Transformerless Grid-Connected PV Inverters," IEEE Transactions on Power Electronics, vol. 29, pp.5358-5369, 2014.
 16. R. Gonzalez, J. Lopez, P. Sanchis, and L. Marroyo,"Transformerless Inverter for Single-Phase Photovoltaic Systems,"IEEE Transactions on Power Electronics, vol. 22, pp. 693-697,2007
 17. X. Huafeng and X. Shaojun, "Transformer less Split-Inductor Neutral Point Clamped Three-Level PV Grid-Connected Inverter,"IEEE Transactions on Power Electronics, vol. 27, pp. 1799-1808,2012
 18. J. S. Lee and K. B. Lee, "New Modulation Techniques for a Leakage Current Reduction and a Neutral-Point Voltage Balancein Transformer less Photovoltaic Systems Using a Three-Level Inverter," IEEE Transactions on Power Electronics, vol. 29, pp.1720-1732, 2014.
 19. Z. Li, S. Kai, X. Yan, and X. Mu, "H6 TransformerlessFullBridge PV Grid-Tied Inverters," IEEE Transactions on PowerElectronics, vol. 29, pp. 1229-1238, 2014
 20. W. Yu, J.-S.Lai, H. Qian, and C. Hutchens, "High-efficiency MOSFET inverter with H6-type configuration for photo voltaic non isolated AC-module applications," IEEE Transactions on Power Electronics, vol. 26, pp. 1253-1260, 2011